

Article

Geochemical Stratigraphy of the *Prima Porta* Travertine Deposit (Roma, Italy)

Mauro Brilli *  and Francesca Giustini 

Istituto di Geologia Ambientale e Geoingegneria (IGAG), Consiglio Nazionale delle Ricerche (CNR), Area della Ricerca di Roma 1, Via Salaria km 29,300, Monterotondo St., 00015 Rome, Italy; francesca.giustini@igag.cnr.it

* Correspondence: mauro.brilli@cnr.it

Abstract: A stratigraphy of a buried travertine deposit was developed using stable isotope geochemistry, trace elements, and radiometric dating. The travertine was identified in a well at *Prima Porta* (north of Rome, Italy), located at the western boundary of the Tiber Valley, a morpho-tectonic depression of extensional origin. It deposited close to a spring that discharged groundwaters from the nearby volcanic aquifer and was associated with the rise of a deep-seated CO₂-rich fluid. The deposition occurred between 53.5 ± 10 ka to 24.2 ± 4.7 ka; its activation was probably coeval with the wettest climatic conditions occurring during Marine Isotope Stage 3, and the end coincided with the cold and arid phase of the last glacial maximum. The chronostratigraphy showed a strong variation in the accumulation rate along the depositional sequence, greater in the lower half and much slower in the upper part, with a sharp decrease in the accumulation rate occurring between 47 and 43 ka. Isotope and chemical stratigraphy described a temporal evolution of events that are correlated to the global climatic variability; palaeoclimatic changes, in fact, influenced the hydrological regime and indirectly the tectonic activity by modulating the emission of deep CO₂, the chemistry of the groundwater, and ultimately the precipitation of the travertine.

Keywords: travertine; stable isotopes; trace elements



Citation: Brilli, M.; Giustini, F. Geochemical Stratigraphy of the *Prima Porta* Travertine Deposit (Roma, Italy). *Minerals* **2023**, *13*, 789. <https://doi.org/10.3390/min13060789>

Academic Editor: János Haas

Received: 30 April 2023

Revised: 6 June 2023

Accepted: 7 June 2023

Published: 8 June 2023



Copyright: © 2023 by the authors. Licensee MDPI, Basel, Switzerland. This article is an open access article distributed under the terms and conditions of the Creative Commons Attribution (CC BY) license (<https://creativecommons.org/licenses/by/4.0/>).

1. Introduction

Along the north-western edge of the Tiber Valley, a morpho-tectonic depression of extensional origin located in the western sector of central Italy, a subterranean travertine deposit named *Prima Porta* travertine (PP), was recently identified in a core recovery from drilling carried out for irrigation purposes. It was studied and described by [1,2]. It is approximately 3 m thick, lying below 8 m of recent alluvial deposits (Figure 1a,b). This travertine was likely deposited in proximity to a spring mainly fed by groundwater which flowed through a volcanic aquifer and was associated with the rise of a deep-seated CO₂-rich fluid.

Previous studies [1,2] aimed to reconstruct the genetic conditions and processes that led to the formation of the PP travertine deposit using stable isotopes, petrographic features, and U-Th dating. They have shown that PP carbonate geobody is a calcitic thermogenic travertine deposited in a low-to-moderate energy environment, such as gently-dipping, shallow pools of low-angle terraced slopes over its entire depositional history, which covered about 30 ka years between the late-stage of Marine Isotope Stage (MIS) 3 and the beginning of MIS 2.

The favorable conditions that led to the deposition of this travertine fit into the context of extensive tectonics, which involved the formation of the largest morpho-tectonic depressions in central Italy, the Tiber Valley. Along this major regional structure, late Quaternary fossil travertines are widespread, as reported in some of the geological literature [3–5]. The travertine development was mostly controlled by two main factors: climate conditions and

tectonic evolution [6,7]. The PP travertine seems to be related mainly to this latter since it formed close to a spring of moderate thermal waters at the western border faults of the graben that housed the paleo-bed of the river Tiber, here oriented NE-SW. It may also have had a climate control because the deposition period (between 54 and 24 ka) encompassed the warm, wet conditions that occurred during MIS 3 and the cold, arid phase of the last glacial maximum, considered climatically adverse to abundant carbonate precipitation when, however, the deposition of travertine ended.

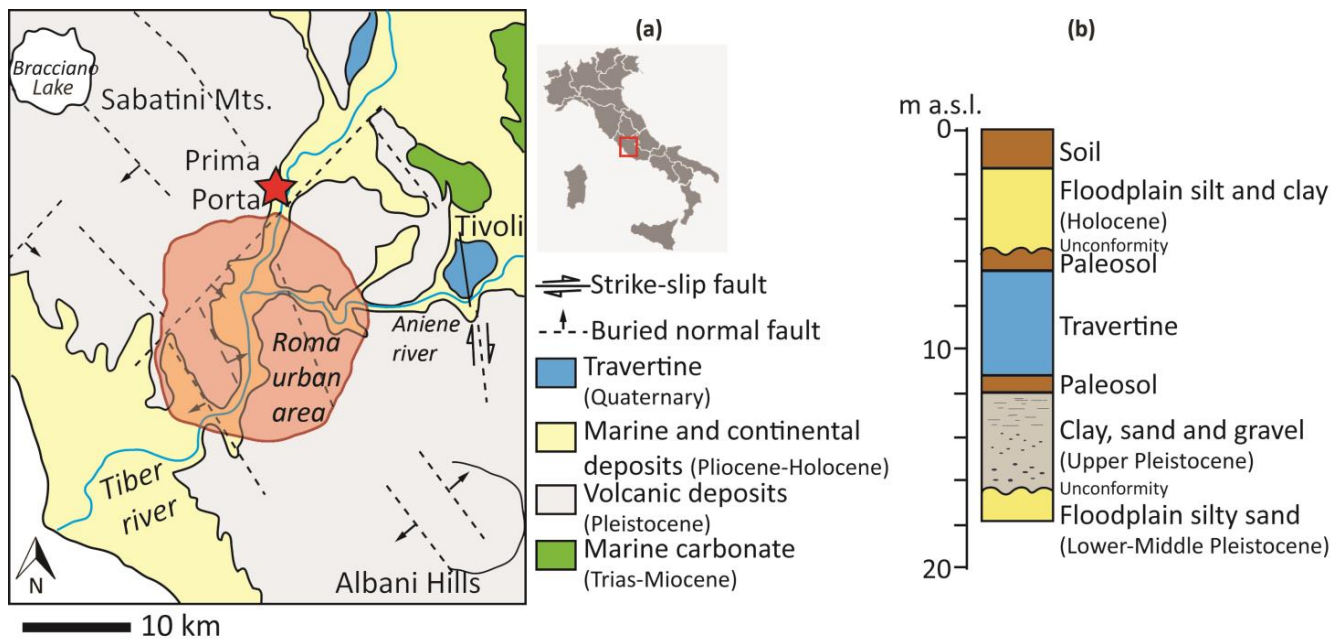


Figure 1. (a) Geological sketch of the *Prima Porta* area and (b) Schematic section of the core (m a.s.l stands for meters above sea level); the travertine deposit (in blue) is set within the alluvial sediment of the river Tiber between two levels of paleosols that mark periods of aridity before and after its formation.

At first glance, the available stable isotope data in [2] did not show interesting paleoclimate-related changes when plotted versus the core recovery depth, nor events that could be related to the structural evolution of the area. To verify whether the palaeoclimatic signal was hidden in the apparent 30 ka continuous sequence, the stratigraphy of some trace elements was developed in this study and paralleled with the isotopic records. A group of elements, generally considered to substitute to different extents for calcium in the crystal lattice of calcite [8], was analyzed by Inductively Coupled Plasma Atomic Emission Spectrometry (ICP-AES) using the same samples used for measuring isotope ratios in [2].

Extracting palaeoclimatic and palaeoenvironmental information from terrestrial carbonate deposits has been largely applied to Quaternary environmental science research; nevertheless, speleothems ([9] and references therein) or lake sediments ([10] and references therein) were used typically for long and detailed palaeoclimatic records, and [11] and references therein also reported as riverine tufa carbonates can preserve palaeoclimatic information in their geochemical records, emphasizing that they offer an opportunity to study details of relatively short-lived climatic events since calcareous tufas occur in nature with a temporal shorter sequence of a higher resolution due to their rapid accumulation. Stable isotopes, however, were the most used environmental and palaeoclimatic geochemical proxies in the time series of continental carbonate sequences (as they are in the marine stratigraphy), to which chemical stratigraphy has been more rarely applied.

In this paper, we aim for the following targets: First, extracting palaeoclimatic and palaeoenvironmental information from travertine sequences, although the thermogenic

nature of these geobodies would lead to arguing that the geochemical features can mainly reflect endogenic processes; Second, evaluating the potential of elemental parameters in travertine stratigraphy and their effectiveness in combination with stable isotopes to infer environmental signals. A multiproxy geochemical approach to sequential carbonate veins deposited by deep, CO₂-rich fluids was successfully used to derive palaeoclimate and fault movement records of the last 135 ka [12].

2. Geology of the Area

The PP travertine is in the lower Tiber Valley to the north of Rome, in the inner sector of the Central Apennine fold-thrust belt, a Meso-Cenozoic carbonate thrust sheet that built up and migrated eastward during the Neogene westward subduction of the Adriatic plate [13]. From the end of the Neogene to the Quaternary, on the Tyrrhenian side of the Apennine belt, extensional back-arc processes have occurred: the reduction of the thickness of the lithosphere, volcanism, extensional basins, and high heat flux [14–19].

Since the Pleistocene (in the last 1.4 Ma), the entire area underwent active uplift [20]. In this period, a juvenile river, the “Paleo-Tiber” [21–24], developed in a palaeo-valley of tectonic origin with a NNW-SSE trend (Paleo-Tiber Graben [25]); the fluvial sedimentation was largely driven by glacio-eustatic sea-level fluctuations [26] and mostly characterized by gravel, sand, and minor amount of mud, deeply entrenched into the Pliocene-Early Pleistocene marine clay and silt [27]. In the middle Pleistocene, about 700 ka, large explosive volcanic activity superimposed fluvial development; it originated from the Albani Hills and Sabatini Mts. and characterized the Roman Area with its peculiar alkaline–potassic eruptive products, remaining intermittently active until recent times [28,29]. The fluvial deposits were covered by thick pyroclastic sequences (ignimbrites, phreatomagmatic ashes, pumice, and ash falls), dating from about 600 to 280 ka [30,31]. This recent tectonic history differs from the previous extensional regime because it is mainly characterized by N-striking right-lateral and NE-striking transtensional-to-normal faults [32,33]. These structures have partially controlled the latest stages of volcanism and related hydrothermal outflows [34]. It is during this phase, characterized by episodic volcano-clastic contributions from the nearby volcanic districts, that the river network changed its original N-S orientation, consistent with the extensional structures, to a transversal direction, wedging its bed between the Albane and Sabatine volcanites.

The PP travertine is placed at the top of the Upper Pleistocene-Holocene fluvial incised valley, which constitutes the Tiber Depositional Sequence ([35] and references therein), a complex stratigraphic architecture that crosscuts the Paleo-Tiber Graben. The valley fill was mostly controlled by the last cycle of sea level change (from MIS 5d to MIS 1) and is composed of basal channel gravels and overlying channel sand and floodplain mud, respectively ascribed to the late lowstand, still regressive phases (26–14 ka) and to the late transgressive, highstand phases (14–0 ka). Buried and detached depositional terraces (locally preserved below more recent deposits) are attributed to the early lowstand phase (116–26 ka) and record intermittent phases of sedimentation during the general lowering of the base level.

In the study area, the alluvial plain is ~2 km wide and has elevations ranging from 19 to 22 m above sea level; to the west and east, the plain connects to slightly higher sectors (up to ~80 m a.s.l.), corresponding to the volcanic hills. The *Prima Porta* borehole is located on the west side of the plain, close to the hilly western sector belonging to the Sabatini volcanic complex (Figure 1a).

Hydrogeology Features

The regional hydrogeology of the area of the Tiber Valley is controlled by stratigraphic sequences and structural settings. Allochthonous, low-permeability Mesozoic-Cenozoic (Upper Cretaceous- Paleogene) flysch sequences, and post-orogenic clay-rich Miocene-Quaternary sediments, overlying Meso-Cenozoic limestones, represent the regional aquiclude [36]. It underlies the Quaternary volcanic and alluvial sediments.

The area of *Prima Porta* lies at the northern border of the Paleo-Tiber Graben. The graben is filled by an aquifer more than 100 m thick towards the southern edge, consisting of a thin layer of volcanic rocks over layers of sand and gravel. [36]. In the north, around the study area, the aquifer thickness is reduced. The presence of numerous springs, mainly located along the eastern side of the valley where the bedrock is shallower than the right bank, marks the lithological contact between Plio-Pleistocene bedrock and sedimentary or volcanic rocks. The springs are often ipothermal and sometimes associated with gas emissions because fluids flow upward along tectonic discontinuities from deep reservoirs. The chemical composition of the related groundwater is generally dominated by Ca, Mg, and SO₄, which is derived from the dissolution of Mesozoic carbonate rocks and a Triassic anhydride layer at the base of the carbonate succession. Some groundwater is enriched in Na and Cl, probably due to the dissolution of Miocene-Pliocene marine evaporates [3,37].

3. The Previous Studies

As reported by [2], the travertine body was found between 8 and 11 m of an about 18 m core drilled on the alluvial sediments of the Tiber Valley. The stratigraphy of the recovery drill is shown in Figure 1b. Below the travertine, a massive, dark brown/red clayey paleosol layer of one meter is followed by 6 m thick of grey, massive pebbly, silty sand and clay with sparse carbonate encrustations, sediments of the Tiber Depositional Sequence [35] that rest unconformably over yellow-beige, massive, silty sands, attributed to the Paleo-Tiber Unit. Above the travertine body, a paleosol again marks a break in the depositional episode, and the upper part of the core consists of beige, massive silts, and clays, which are associated with a floodplain environment; they likely record the most recent phase of deposition from overbank flooding of the Tiber River. The travertine is white and characterized by horizontal to sub-horizontal, irregular, wavy laminations, with alternating dm-thick planar bedsets and sub-horizontal bedlets; the macro and microscopic observations evidenced a quite repetitive alternation of undulated layers of rafts and shrubs between micrite crusts, which macroscopically are substantiated by the sub-horizontal, irregular, wavy laminations; these structures can be reconducted to a typical low to moderate energy genetic environments, such as terrace pools or flat ponds. Only in 15 cm out of the entire thickness are the depositional surfaces steeply inclined (up to 45° dip), in the interval between 10.15 and 10.30 m depth, indicating that at that position, a slope system, such as the rims and walls of pools in terraced slope dams, has taken place for a certain elapse of time. With such exceptions, it is possible to argue that along the vertical profile of the travertine, the environmental setting did not substantially change during its development, likely remaining subaqueous and devoid of erosional surfaces.

Stable isotopes of carbon and oxygen from 17 samples collected randomly along the travertine sequence were also analyzed by [2], allowing the further definition of the genetic constraints and evidencing the origin of carbon and the environmental temperature (the isotopic data published in [2] are also listed in Table 1). The high $\delta^{13}\text{C}$ signature, between +8.8 and +11.2‰, reflects non-soil carbon sources and an origin likely associated with the decarbonation of local carbonate bedrock; the $\delta^{18}\text{O}$ range is consistent with a carbonate precipitated from water with an isotopic composition close to that of the present-day local groundwater and temperatures between 8 and 17 °C [38]. The local groundwater, sampled in the well from which the core was drilled, showed a pH between 5.9 to 6.2, conductivity between 3080 and 2752 $\mu\text{S}/\text{cm}$, and temperatures between 18 and 20 °C (data measured at different periods of the year, November 2012 and March 2013—these data were partially published in [1]). The discrepancy between the actual water temperature and the calculated one can be attributed to the distance between the location of the drilling and the now undetermined spring orifice. Therefore, the carbonate-precipitating water may have cooled due to surface flow.

Table 1. Elemental composition, stable isotopes, U/Th ages, and depth of the samples from PP travertine core. (Stable isotope data and U/Th ages are from [2]).

Sample	Depth (m)	$\delta^{13}\text{C}$ (‰)	$\delta^{18}\text{O}$ (‰)	Fe (ppm)	K (ppm)	Mg (ppm)	Mn (ppm)	Na (ppm)	Sr (ppm)	Age (ka)
TR8 C	7.90	11.84	−3.30	577	819	3710	1291	913	1027	
TR8 E	7.98	11.42	−3.29	477	961	4184	1480	1151	1133	
TR9 C	8.08	10.57	−3.11	752	809	3694	1637	912	850	24.2
TR9 L	8.38	11.65	−3.37	449	1019	3765	1775	1167	1201	
TR9 P	8.55	11.26	−3.25	474	934	3909	1593	1042	894	44.6
TR9 U	8.76	11.24	−3.6	638	830	2947	1395	908	727	
TR9 X	8.84	11.54	−3.41	586	706	2370	1127	672	478	
TR9 Z	8.97	11.06	−3.06	678	667	2463	1551	656	432	
TR10 C	9.10	10.81	−3.15	740	665	2197	1287	656	459	
TR10 E	9.18	10.38	−3.54	491	668	2107	1247	630	445	
TR10 F	9.23	10.83	−3.32	508	656	2248	1179	624	439	50.4
TR10 H	9.32	10.61	−3.16	612	638	1805	1271	593	315	
TR10 O	9.54	11.00	−3.30	590	677	2364	953	667	350	
TR11 G	10.07	11.54	−2.93	541	672	2671	1239	716	336	
TR11 M	10.35	11.52	−2.88	604	700	2992	1176	736	361	53.5
TR11 P	10.46	11.22	−3.08	694	774	2493	1392	757	339	
TR11 R	10.53	11.82	−2.66	790	712	3360	1047	767	412	

The most striking aspect of the isotopes of this travertine is the complete absence of any correlation between the two variables (Figure 2a); this suggests that the environmental conditions remained stable throughout formation unless a thorough diagenetic isotope resetting did involve the entire carbonate body after the completion of deposition. Ref. [2] detected the effects of diagenesis in the secondary deposition of cement only, although not very frequent; some microfractures filled by sparite crystals and re-crystallization forming darker micrite surrounded by cloudy micrite or sparite crystals were observed. These cements were randomly analyzed for stable isotopes; they resulted similarly or identically to the primary calcium carbonate as if it may be constituted by early diagenetic fabrics connected to syn-sedimentary fluids. Post-depositional precipitation of sparry calcite within the porosity was revealed in a singular case by the total carbon isotope reset due to organic carbon incorporation. The largely maintained depositional pore network and the absence of primary precipitation of aragonite suggest that post-depositional dissolution and reprecipitation events did not occur on a large scale; finally, considering that (i) the quantity of cement that lines the voids and pores is quite limited and, (ii) the isotope composition of the cement is similar to that of the bulk rock and micrite samples in most cases, cementation probably did not cause a significant diagenetic resetting of the isotope signature. Instead, re-crystallization is generally considered a process relating to early diagenesis [39] or a syn-depositional process [40]. In these cases, it is reasonable to assume that circulating fluids had the same characteristics (e.g., temperature and $\delta^{18}\text{O}$) as the water from which carbonate precipitation occurred and, therefore, the observed re-crystallization had no significant impact on the isotope ratios.

U/Th dating of the travertine of four approximately equally spaced levels yielded the following ages: 53.5 ± 10 ka, 50.4 ± 8.7 ka, 44.6 ± 6.4 ka, and 24.2 ± 4.7 ka, which were respectively placed at 10.35, 9.23, 8.55, 8.08 m from the top of the core (data already published in [2] and reported in Table 1). The deposition history of the travertine deposit encompassed a period of great climatic variability (intercepting both the MIS 3 and the MIS 2) within a general cooling trend which had its peak at the last glacial maximum.

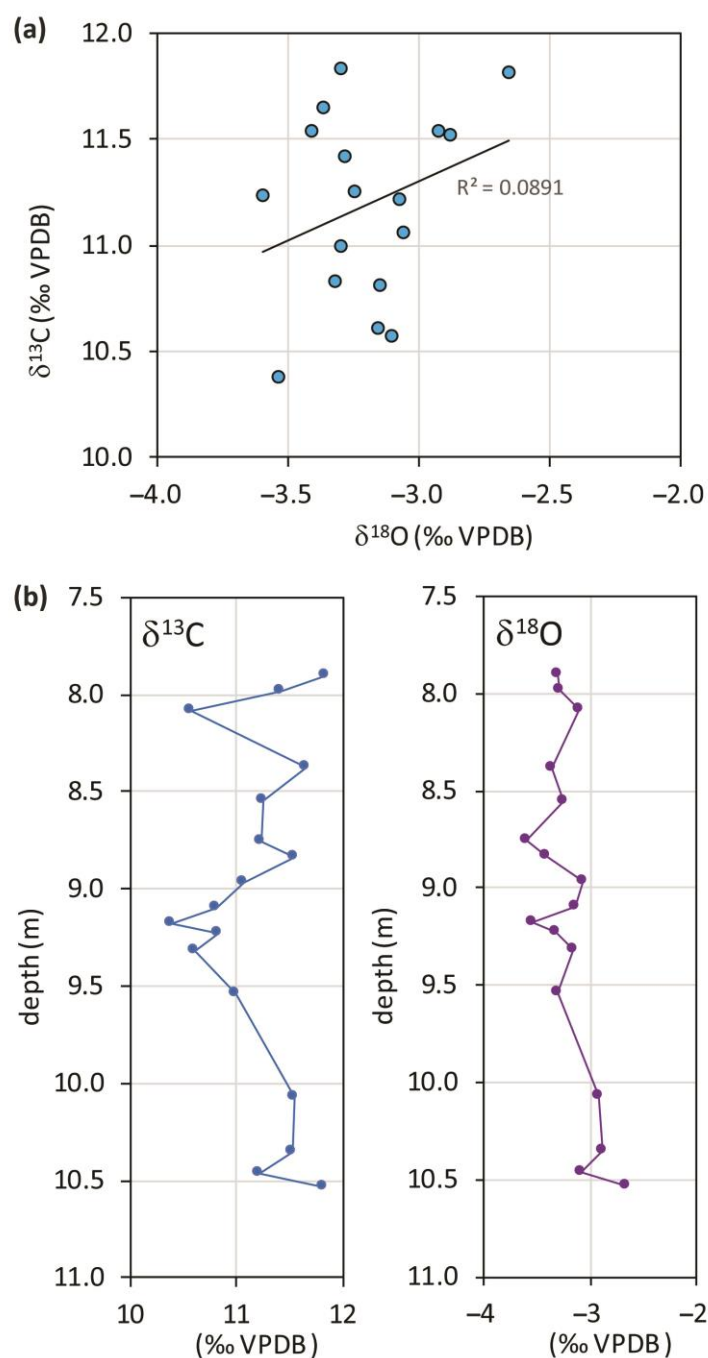


Figure 2. (a) Scatterplot of stable oxygen and carbon isotope compositions from *Prima Porta* travertine samples, data are from [2]; (b) $\delta^{13}\text{C}$ and $\delta^{18}\text{O}$ profiles of the travertines of *Prima Porta* versus depth of recovery.

4. Sampling and Analytical Method

Sampling was described by [2]. On the 17 samples in which stable isotope ratios were determined, the concentrations of Sr, Mn, Mg, Fe, Na, and K were analyzed by ICP-AES with a Varian Vista RL CCD Simultaneous ICP-AES spectrometer with an axial torch (Department of Earth Sciences, Sapienza University, Rome, Italy).

A 3% solution of hydrochloric acid (HCl) was added at room temperature to about 200 mg of each powdered sample and maintained under stirring. The acid was introduced in successive small additions while monitoring the pH. Upon completion of the acid-carbonate reaction, after about 1 h, the solution was filtered (0.2 μ). Following the

principles described by [41], this approach aimed to minimize the dissolution of cations from silicate impurities in the bulk carbonate sample, whereas oxide compounds were at least partially dissolved. All solvents and reagents were of the highest purity grade commercially available. Deionized water (resistivity $18 \text{ M}\Omega \text{ cm}^{-1}$) obtained from a Milli-Q purification system was used to prepare all standard and sample solutions that were eventually analyzed by the ICP instrument. Emission lines for ICP-AES analysis were chosen according to previous interference studies. Internal standards were added to compensate for any effects from acid or instrument drift. Analytical precision was calculated as the percent relative standard deviation of a set of ten repetitions of the same sample of travertine calcite in any single session of analysis. Results indicated precision values always less than 5% for Sr, Fe, K, and Na elements, of which the concentrations were between 2 and 5 mg/L in the sample digestion acidic solutions; always less than 3% for Mg and Mn which were between 5 and 20 mg/L. Accuracy was evaluated on standard solutions and was less than 10% for all elements. The measurement conditions and emission lines are listed in Tables A1 and A2 of the Appendix A.

5. Results

As already determined in [1,2], the PP travertine is totally calcite, with no relics of aragonite crystal structures (radiated fibers or needle aggregates) upon observation of thin sections. The mineralogy of the CaCO_3 phase is the prime factor determining the concentration of a trace element in its lattice [8].

Table 1 shows the results of the chemical analysis together with the results of isotopic analysis and U/Th dating.

Covariation plots of travertine chemistry allow us to establish when the presence of cations is related to a common process that, for Sr and Mg, is dominantly the substitution for Ca in the calcite crystal lattice. Figure 3 shows that these two elements are strongly, positively correlated. Na and K are strongly positively correlated with each other and, in turn, correlated with Mg and Sr. All these elements seem to mainly be substitutes for Ca. Since their behavior is essentially in agreement and since it is reasonable to assume that their partition coefficients between water and solid phase respond differently to temperature, deposition rate, and salinity, it is possible to conclude that their abundance is mainly related to the respective concentrations in the travertine-precipitating waters. Consequently, the elemental variations as a function of time reflect the different rates of silicate mineral dissolution from the volcanic aquifer.

Whereas iron is definitely uncorrelated with other cations, Mn shows intermediate behavior. It must be concluded that iron may represent a detrital fraction present in the travertine or a residual component, made of oxides and hydroxides and produced during travertine deposition or post-syn-sedimentary travertine dissolution; manganese is a mix between the calcite crystal lattice incorporation and other provenances.

Chemical data, when stratigraphically plotted versus depth (Figure 4), show common features, as obvious for the highly correlated elements (Mg, Sr, Na, K). These trends can be summarized as low concentration levels in the lower section, between 10.5 and 9.3 m, and an apparent gradual increase towards the top. For Mn, this trend is barely visible, and it is absent for iron.

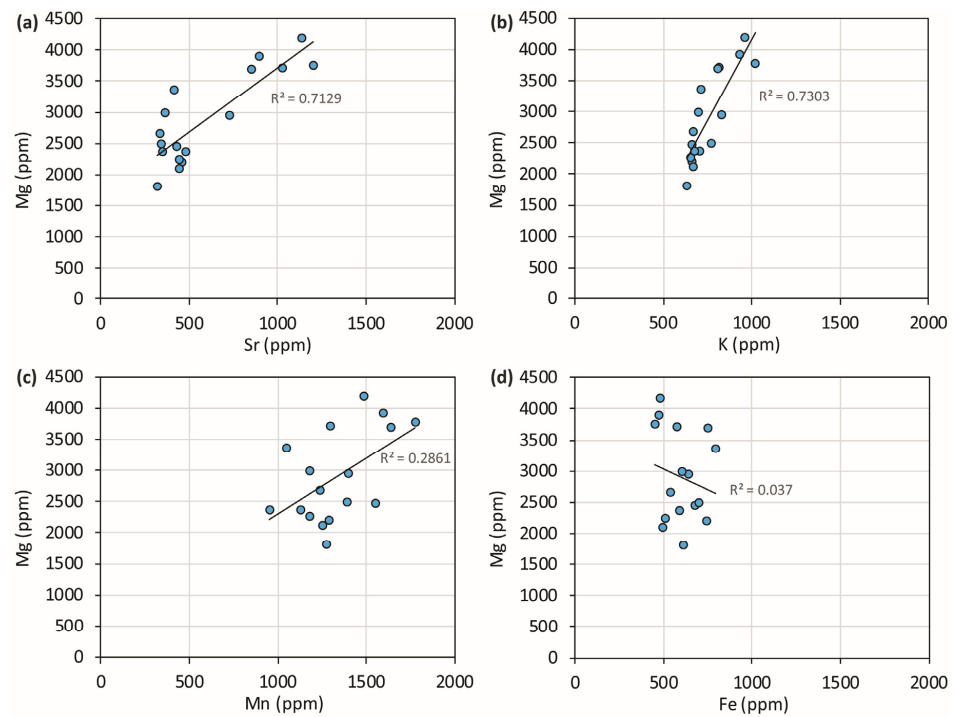


Figure 3. Covariation plots of PP travertine chemistry. Sr and K are strongly correlated with Mg and, in turn, are strongly correlated. Na is not presented in these scatterplots as it behaves similarly to K.

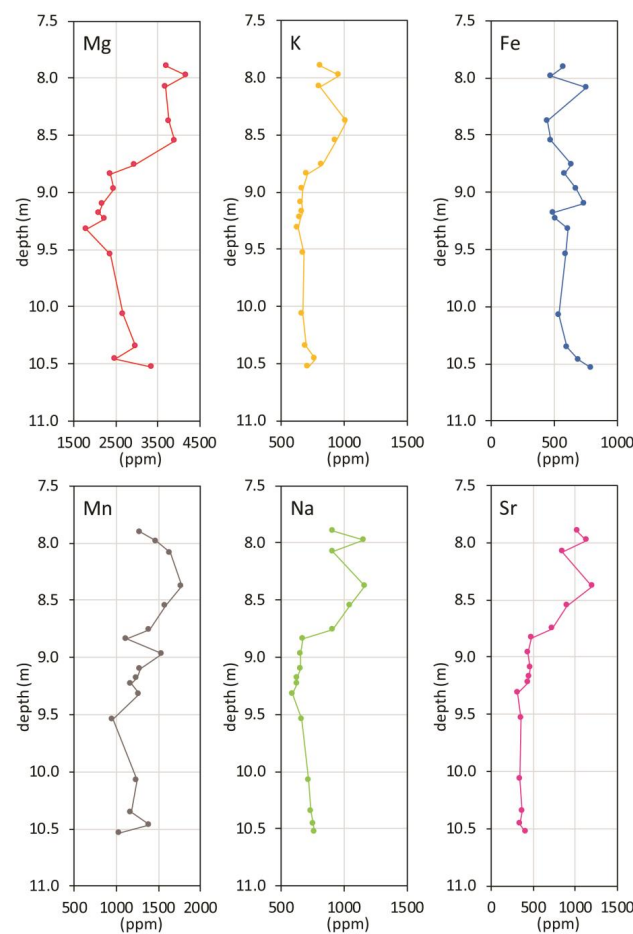


Figure 4. Chemical data plotted versus depth.

6. Discussion

Minor and trace elements Sr, Mn, Mg, Fe, Na, and K were analyzed as they can potentially substitute, to varying degrees, for Ca in the CaCO_3 (calcite) crystal lattice. Sr and Mg were selected because they are abundant and the most common substitutes for Ca. The partition of Mg between calcite and water has been extensively studied in marine solutions, and it depends on several factors; nevertheless, in freshwater environments with low ionic strength and low Mg/Ca ratios (<1), it is possible to argue that its content in the calcite precipitates is determined only by the Mg/Ca ratio and the temperature of the parental water [42,43]. The variations in Mg content observed in the PP travertine may be partly due to temperature changes. Still, its strong correlation with Sr, whose behavior as a function of temperature is generally irrelevant [44,45], suggests that the main factor for forcing the Mg and Sr variations is their content fluctuation in the water. Na and K incorporation is thought to occur predominantly by substitution for Ca, as the correlation with Sr and Mg would indicate; this substitution occurs with a charge imbalance that had to be compensated by further chemical substitution. Their abundant presence in the travertine (on average 800 and 750 ppm) indicates that travertine parental groundwater largely interacted with the aquifer of the nearby Sabatini volcanic complex, one of the largest centers of the alkali potassium Roman volcanic province. The water chemistry reported by [1] measured at the PP well also shows a high concentration of Na and, especially, K (146 and 203 mg/L, respectively). Finally, iron and manganese, which in principle can substitute for Ca in the calcite lattice, as Fe (II) and Mn (II), do not seem to have this provenance, as they are uncorrelated with the other elements. Their presence in the aqueous solutions that precipitate the PP travertine could be relatively abundant as the field parameters measured in local groundwater in different periods show slightly reducing features and a pH around 6; after the emergence, the presumable progressive transition to oxidative features of these waters may have led to the oxidation of iron and its precipitation as insoluble oxides and hydroxides (when it is not already precipitated as insoluble FeCO_3); whereas Mn (II), which is stable at this oxidation state in natural surface environments, is likely precipitated as MnCO_3 even if a certain possibility of incorporation into the calcite crystal lattice cannot be totally excluded. Furthermore, iron may also have concentrated in residual products after post- or syn-sedimentary processes of travertine compaction and dissolution. The same fate may have involved Mn, given the difference of several orders of magnitude in the solubility product between calcite and rhodochrosite mineral phases [46]. Since the acid attack used for the analysis can dissolve both the oxide and the carbonate phases, the results likely reflect the cationic substitutes of the calcite and the sedimentary residual fractions. The results of the iron and manganese contents may have been affected by the latter components.

6.1. PP Travertine Chrono-Stratigraphy

Using the four U/Th dates, an age model was drawn and shown in Figure 5a. The points, representing ages versus depths, have been linearly interpolated, and consequently, a constant accumulation rate is assumed; it is displayed, expressed in centimeters per thousand years, as a three-stepped line in Figure 5b. This representation has the evident drawback of introducing artificial discontinuities in the sedimentation rate but the advantage of making evident the remarkable difference between the bottom and the top of the travertine sequence. Simple calculations allow us to estimate that after the first 10 ka, the average accumulation rate varied from 35 to 12 cm/ka, whereas in the last 20 ka, it dropped by one order of magnitude, on average, to 2.4 cm/ka. It is evident that most of the travertine was deposited on terraced sediments between 55 and 45 ka; from 45 ka onwards, the precipitation was still active until at least 24 ka and potentially until 16 ka, but at a considerably slower rate; the upper 50 cm have the longest duration, exceeding 20 ka. The period over which the PP travertine formed corresponds to MIS 3 (57–29 ka) and part of MIS 2 (29–14 ka) [47]. Climatically, this period was characterized by considerable variability; millennial-scale Dansgaard–Oeschger (DO) cycles (abrupt temperature rise

followed by gradual cooling) [48,49], episodically interrupted by cold phases (Heinrich events), superimposed on a cooling trend which culminated in the last glacial maximum (LGM) (26.5–19 ka) [50], when the global ice volume reached its maximum expansion and the eustatic sea level was at its lowest.

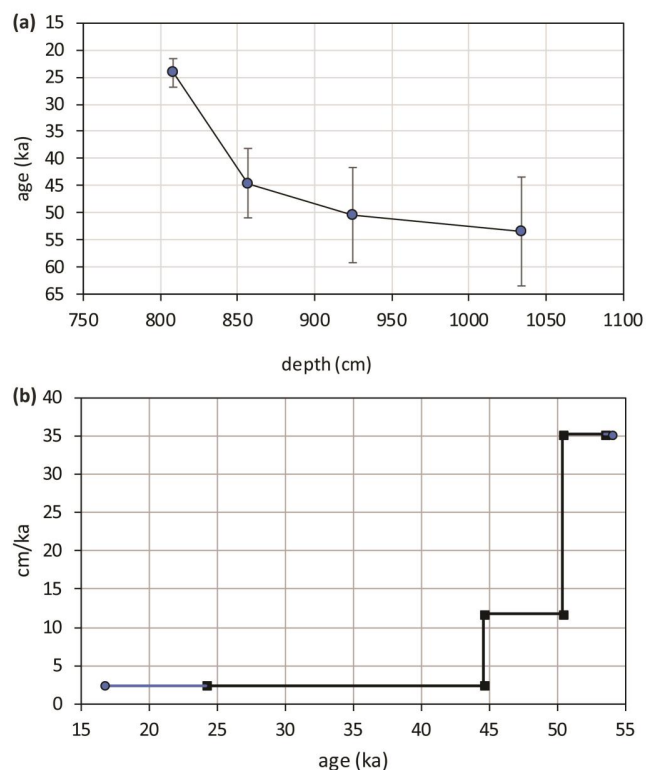


Figure 5. (a) Age model developed from the U/Th ages and the depths of the samples which were measured for U/Th dating technique, age model dots have been linearly interpolated; (b) Accumulation rate of PP travertine derived from the age model (blue prolongations of the line represent the linear extrapolation of accumulation rate outside the measured age interval).

The age model allowed the conversion of the chemical and isotopic data from the depth to the time domain (Figure 6). The elemental records versus time are clearly similar (Figure 6), except for iron (not reported in the figure). Concentrations in ppm show lower values between the 55 and 45 ka interval, after which a sudden positive shift is evident. The duration of the shift is about 4 ka. Hereafter the curves maintain a constant trend up to 16 ka, which marks the end of travertine deposition according to the linear extrapolation of the accumulation rate. The oxygen isotopes behave concordantly with the Ca-substitute elemental profiles: they show a decline in the 55–47 ka interval and a steady state after 43 ka; the variations recorded by the isotopic curve are very limited and are always less than one delta unit.

Referring to the detailed Greenland ice core data record (NGRIP) of global-scale climate evolution during the period of formation of the PP travertine sequence, it is possible to correlate the lower end of the sequence with the sharp climatic amelioration that took place at 54 ka coinciding with Dansgaard–Oeschger (DO)-14. This climatic event could mark the onset of PP deposition; the subsequent cooling trend of the DO cycle could be found in the concave profile of some PP records, such as those of Mg and isotopes. The upward recovery of the curves and the termination of this interval coincide perfectly with the abrupt temperature increase related to DO-12 at 46.5 ka. In this perspective, the oxygen isotope record can be interpreted to reflect the oscillation of oxygen isotopes in the precipitation waters that fed the local aquifer, and the variability in the calcite elemental concentrations must therefore reflect the variation of the ratio of trace elements to calcium (X/Ca ratio) in the groundwater. From the 47 ka onwards, the NGRIP record shows successive DO-

cycles superimposed to a general trend leading to the LGM; the last 26 ka recorded in the travertine data have a much minor time resolution due to the dramatic fall in the accumulation rate, inferior to the minimum to detect the next climatic oscillations. The general trend does not allow for even the identification of the LGM. It shows a slight decrease in elemental concentrations of Ca-substitutes, especially evident for Sr, and a slight negative peak for $\delta^{13}\text{C}$.

The palynological signature for the last 300 ka from the Valle di Castiglione site [51], only about 25 km southeast of the PP travertine location, marked major local vegetation events that can be correlated with global climate change. The curve in Figure 6 represents one aspect of the processing of palynological data: the ratio (in percentage) between arboreal and non-arboreal pollens, which provides a record of humidity evolution. The positive peaks can be interpreted as corresponding to relatively humid times (more arboreal pollens), whereas depressions represent relatively dry times (less arboreal pollens). In the development period of the PP travertine, the pollen record shows a decrease in humidity from a peak placed before the onset of PP deposition (not shown in the figure); within the interval between 54 and 47 ka, a rise of humidity and its successive decline is apparent (Figure 6). After the period when the maximum development of PP travertine ends, the pollen recorded its driest conditions, which, aside from episodic weak recoveries, remained stable until the LGM.

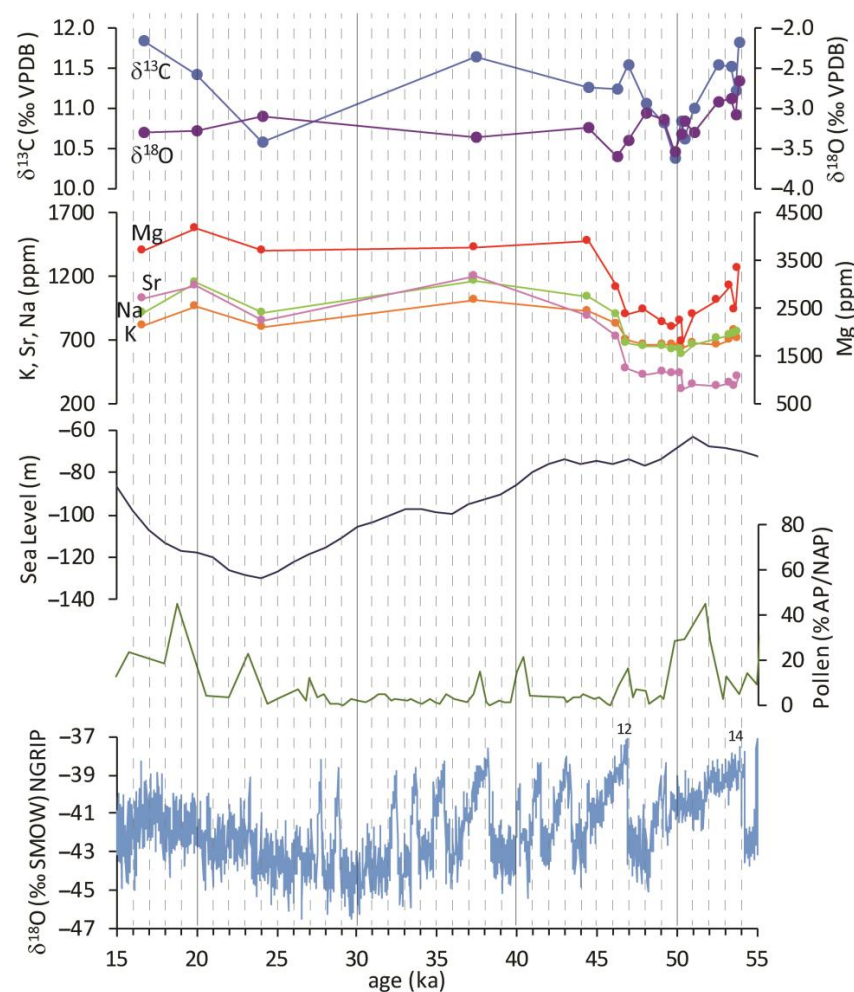


Figure 6. Comparison of different palaeoclimatic records between 15 and 55 ka. From the top: isotopic records of PP travertine; alkali and alkaline earth metal records expressed in ppm of PP travertine; sea level change from [52]; arboreal to non-arboreal pollens ratio expressed in percentage from [51]; NGRIP $\delta^{18}\text{O}$ record (numbers represent the DO events) from [48].

6.2. Climate Evolution in PP Travertine Records

The climatic evolution described by the Greenland ice core data record [48], Valle di Castiglione palynological stratigraphy [51], and sea level record from [52], displayed in the lower half of Figure 6, has influenced the chemistry of the PP travertine-precipitating groundwater. The variations in all elemental and isotopic records can be traced to variations in climatic changes on a global scale, as the correlation with the NGRIP record, especially between 54 and 43 ka, would demonstrate. The cooling event after DO-14, which started at 54 ka, was recorded in the oxygen isotope record as a decrease in $\delta^{18}\text{O}$ of precipitation waters; it was, however, a period of relatively high humidity. The $\delta^{13}\text{C}$ record has a trend concordant with the $\delta^{18}\text{O}$ record showing an inflection that is expected to reflect either a decrease in spring CO_2 outgassing related to atmospheric cooling or a decrease in the deep CO_2 component of the gas emission, the latter leading, in turn, to an increased contribution of more negative soil CO_2 . After 50 ka, both isotopic records showed a modest recovery as if to restore the initial conditions. However, the superimposed trend of climatic deterioration that led to the glacial phase created cold/arid conditions and a progressive decrease in sea level, which resulted in a reduction in the availability of groundwaters. The alkali and alkaline earth metal records showed little to no change at the first cooling as a mostly humid interglacial climate persisted. It evidently caused only a decrease in Mg/Ca ratios in groundwater or a possible temperature-dependent decrease in partition coefficient. At about 48 ka, when the oxygen record stabilizes at its lowest level (around -3.3‰), all elemental concentrations show a sudden shift to higher values. Minerals containing Ca have greater resistance to weathering due to water-rock interaction, so this shift reflects a greater dissolution of metals from volcanic aquifer rocks relative to Ca. A decrease in water aggressiveness to the aquifer rocks can be inferred. The increase in X/Ca ratios in groundwater can be interpreted as a result of the increasing pH due to a reduction of the deep CO_2 input at the shallower crustal levels. This event may have followed a change in the hydraulic conductivity related to a fracture restriction driven by locally reduced pore pressure resulting from decreased groundwater recharge. The reduction of CO_2 surface emission reduced the input of carbon from deep sources, and the lowering of the regional water table greatly influenced water availability; both events dramatically reduced the precipitation rate of the PP travertine.

7. Conclusions

A recent study on the product of drilling carried out on the right bank of the Tiber River Valley, immediately northeast of Rome (*Prima Porta*), revealed the presence of a 3 m thick travertine body lying below 8 m of alluvial deposits. It was studied for isotope and chemical stratigraphy and U/Th dating. This travertine was deposited near a spring fed by groundwaters from the volcanic aquifer of the Sabatini mountains. It was associated with the rise of thermal, CO_2 -dominated fluids from the deep crust through direct faulting related to the graben hosting the Tiber Valley. U/Th dating has shown that this travertine body was formed in the period 55–16 ka, and that about 46 ka ago, the accumulation rate of the travertine sequence recorded a sharp decline. Age data from *Prima Porta*, although having a high level of uncertainty, suggest that travertine deposition started approximately coeval with the wettest/high-temperature conditions of the DO-14 event, whereas the end of deposition would coincide with the cold and arid phase of the LGM. Isotope records of the travertine layers described a palaeoclimate coherent to this evolution, even if the signal cannot be interpreted from 43 ka onwards because of the reduced sampling resolution. Chemical records seem to reflect the element variations (at least for those which substitute for Ca in the travertine calcites) in the travertine-precipitating groundwaters: after an approximately constant level in the 55–47 ka interval, a remarkable shift towards higher content occurred lasting about 4 ka; this shift was coeval with the accumulation rate reduction and with the definitive establishment of arid and cold climatic conditions. After this event, the elemental records remain steady until the top of the sequence. This event has a remarkable palaeoclimate connotation as shown by its correlation with the

following events: (i) the abrupt temperature increase that marks the DO-12 at 46.5 ka and its subsequent descent, (ii) the end of the warm, humid peak registered by pollen record of Valle di Castiglione, (iii) the onset of a definite sea level decrease (and a climate trend that led from MIS3 to MIS2 and to the LGM). Its clearest evidence in the chemical records and accumulation rate rather than in isotopes is because this event is related to effects that have had a strong impact on the hydrological system. The relatively rapid settling down of the glacial and arid climate triggered a series of events resulting from the lowering of the regional aquifer water table. The decrease in water availability caused a reduction in the hydrostatic pressure and fracture openings in the crust; this may have contributed to changing the hydraulic conductivity of the faults with a consequent reduction of CO₂ input into the groundwater, which became less aggressive towards the rocks of the aquifer; the reduced dissolving capacity of the groundwater changed its chemistry which was recorded in the carbonates deposited upon its emergence.

The establishment of glacial and arid climatic conditions, therefore, had simultaneous effects on the groundwater level and the fault movements, with consequences on the depositional–erosive process of the PP travertine.

This paper demonstrates the efficacy of a multimethod approach, using trace elements in combination with isotopes and dating techniques, to address the difficulties of untangling the palaeoclimatic signals present in travertine deposits. These are continental sedimentary geo-bodies often scarcely considered for palaeoclimatic investigation compared to speleothems (or calcareous tufas) because they are endogenous and, therefore, less influenced by surface environments. Nevertheless, the information they provide can be even more organic if we want to deduce the evolution of the climate together with its interaction with the earth and the environmental dynamics.

Author Contributions: Conceptualization, M.B. and F.G.; methodology, M.B. and F.G.; investigation, M.B. and F.G.; writing—original draft preparation, M.B.; writing—review and editing, M.B. and F.G. All authors have read and agreed to the published version of the manuscript.

Funding: This research was funded by the project of Italian CNR: DTA.AD002.707–Lab. Isotopi Stabili (Coordinator M. Brilli).

Data Availability Statement: All data are available in the article.

Acknowledgments: We sincerely thank Azienda Agricola Orti del Canottiere, Giuseppe Capelli, and Livio Manzetti for providing a travertine core and permitting access to the study area. We also thank the technician of the ICP-AES lab Teodoro Coppola of the Department of Earth Science of the Sapienza University of Rome, for the assistance in the analysis. We are indebted to Asmaa Fayek of Helwan University, Cairo, Egypt, for her continuous help in the laboratory work.

Conflicts of Interest: The authors declare no conflict of interest.

Appendix A

Table A1. Main operating conditions for ICP-AES analysis.

RF power	1.3 kW
Gas	Ar 99.999%
Plasma Ar flux	16.5 L min ^{−1}
Auxiliary Ar flux	1.5 L min ^{−1}
Nebulizer Ar flux	0.70 L min ^{−1}
Sample aspiration rate	1 mL min ^{−1}
reading	30 s
number of replicates	3

Table A2. Analytical characteristics of the ICP-AES method.

	λ [nm]	LOD * [mg kg ⁻¹]
Na	589.592	2
K	766.490	4
Ca	396.847	0.06
Mg	279.553	0.04
Fe	259.940	0.8
Mn	257.610	0.08
Sr	407.771	0.05

* LOD Limit of detection (3s detection).

References

- Giustini, F.; Brilli, M.; Mancini, M. Geochemical study of travertines along middle-lower Tiber valley (central Italy): Genesis, palaeo-environmental and tectonic implications. *Int. J. Earth Sci.* **2018**, *107*, 1321–1342. [\[CrossRef\]](#)
- Giustini, F.; Brilli, M.; Di Salvo, C.; Mancini, M.; Voltaggio, M. Multidisciplinary characterization of the buried travertine body of Prima Porta (Central Italy). *Quat. Int.* **2020**, *568*, 65–78. [\[CrossRef\]](#)
- Minissale, A.; Kerrick, D.M.; Magro, G.; Murrell, M.T.; Paladini, M.; Rihs, S.; Sturchio, N.C.; Tassi, F.; Vaselli, O. Geochemistry of Quaternary travertines in the region north of Rome (Italy): Structural, hydrologic and paleoclimatic implications. *Earth Planet. Sci. Lett.* **2002**, *203*, 709–728. [\[CrossRef\]](#)
- Mancini, M.; Girotti, O.; Cavinato, G.P. Il Pliocene e il Quaternario della Media Valle del Tevere (Appennino Centrale). *Geol. Rom.* **2004**, *37*, 175–236.
- Manfra, L.; Masi, U.; Turi, B. La composizione isotopica dei travertini del Lazio. *Geol. Rom.* **1976**, *15*, 127–174.
- Faccenna, C.; Soligo, M.; Billi, A.; De Filippis, L.; Funicello, R.; Rossetti, C.; Tuccinei, P. Late Pleistocene depositional cycles of the lapis Tiburtinus travertine (Tivoli, Central Italy): Possible influence of climate and fault activity. *Glob. Planet. Chang.* **2008**, *63*, 299–308. [\[CrossRef\]](#)
- De Filippis, L.; Faccenna, C.; Billi, A.; Anzalone, E.; Brilli, M.; Özkul, M.; Soligo, M.; Tuccimei, P.; Villa, I.M. Growth of fissure ridge travertines from geothermal springs of Denizli basin, western Turkey. *Geol. Soc. Am. Bull.* **2012**, *124*, 1629–1645. [\[CrossRef\]](#)
- Veizer, J. Chapter 8. Trace elements and isotopes in sedimentary carbonate. In *Carbonates: Mineralogy and Chemistry*; Reeder, R., Ed.; De Gruyter: Berlin, Germany; Boston, MA, USA, 1983; pp. 265–300.
- McDermott, F. Palaeo-climate reconstruction from stable isotope variations in speleothems: A review. *Quat. Sci. Rev.* **2004**, *23*, 901–918. [\[CrossRef\]](#)
- Leng, M.J.; Marshall, J.D. Palaeoclimate interpretation of stable isotope data from lake sediment archives. *Quat. Sci. Rev.* **2004**, *23*, 811–831. [\[CrossRef\]](#)
- Andrews, J.E. Palaeoclimatic records from stable isotopes in riverine tufas: Synthesis and review. *Earth Sci. Rev.* **2006**, *75*, 85–104. [\[CrossRef\]](#)
- Kampman, N.; Burnside, N.M.; Shipton, Z.K.; Chapman, H.J.; Nicholl, J.A.; Ellam, R.M.; Bickle, M.J. Pulses of carbon dioxide emissions from intracrustal faults following climatic warming. *Nat. Geosci.* **2012**, *5*, 352–358. [\[CrossRef\]](#)
- Boccaletti, M.; Ciaranfi, N.; Cosentino, D.; Deiana, G.; Gelati, R.; Lentini, F.; Massari, F.; Moratti, G.; Pescatore, T.; Ricci Lucchi, F.; et al. Palinspastic Restoration and Paleogeographic Reconstruction of the Peri-Tyrrhenian Area during the Neogene. *Palaeogeogr. Palaeoclimatol. Palaeoecol.* **1990**, *77*, 41–50. [\[CrossRef\]](#)
- Funicello, R.; Locardi, E.; Parotto, M. Lineamenti geologici dell'area sabatina orientale. *Boll. Soc. Geol. Ital.* **1976**, *83*, 831–849.
- Barchi, M.; Minelli, G.; Piali, G. The CROP 03 profile: A synthesis of results on deep structures of the Northern Apennines. *Mem. Soc. Geol. Ital.* **1998**, *52*, 383–400.
- Jolivet, L.; Faccenna, C.; Goffé, B.; Mattei, M.; Rossetti, F.; Brunet, C.; Storti, F.; Funicello, R.; Cadet, J.P.; D'Agostino, N.; et al. Midcrustal shear zones in postorogenic extension: Example from the northern Tyrrhenian Sea. *J. Geophys. Res.* **1998**, *103*, 12123–12160. [\[CrossRef\]](#)
- Chiodini, G.; Cardellini, C.; Amato, A.; Boschi, E.; Caliro, S.; Frondini, F.; Ventura, G. Carbon dioxide Earth degassing and seismogenesis in central and southern Italy. *Geophys. Res. Lett.* **2004**, *31*, L07615. [\[CrossRef\]](#)
- Acocella, V.; Funicello, R. Transverse Systems along the Extensional Tyrrhenian Margin of Central Italy and Their Influence on Volcanism. *Tectonics* **2006**, *25*, TC2003. [\[CrossRef\]](#)
- Billi, A.; Tiberti, M.M.; Cavinato, G.P.; Cosentino, D.; Di Luzio, E.; Keller, J.V.A.; Kluth, C.; Orlando, L.; Parotto, M.; Praturlon, A.; et al. First results from the CROP-11 deep seismic profile, central Apennines, Italy: Evidence of mid-crustal folding. *J. Geol. Soc. Lond.* **2006**, *163*, 583–586. [\[CrossRef\]](#)
- Mancini, M.; D'Anastasio, E.; Barbieri, M.; De Martini, P.M. Geomorphological, paleontological and ⁸⁷Sr/⁸⁶Sr isotope analyses of Early Pleistocene paleoshorelines to define the uplift of Central Apennines (Italy). *Quat. Res.* **2007**, *67*, 487–501. [\[CrossRef\]](#)

21. Funciello, R.; Giuliani, R.; Marra, F.; Salvi, S. The influence of volcanism and tectonics on Plio-Quaternary regional landforms in the Southeastern Sabatinian area (Central Italy). *Mem. Descr. Carta Geol. d'It.* **1994**, *49*, 323–332.
22. Marra, F.; Rosa, C.; De Rita, D.; Funciello, R. Stratigraphic and tectonic features of the Middle Pleistocene sedimentary and volcanic deposits in the area of Rome (Italy). *Quat. Int.* **1998**, *47*, 51–63. [[CrossRef](#)]
23. Giordano, G.; Esposito, A.; De Rita, D.; Fabbri, M.; Mazzini, I.; Trigari, A.; Rosa, C.; Funciello, R. The sedimentation along the Roman coast between Middle and Upper Pleistocene: The interplay of eustatism, tectonics and volcanism. New data and review. *Il Quat.* **2003**, *16*, 121–129.
24. Girotti, O.; Mancini, M. Plio-Pleistocene stratigraphy and relations between marine and non-marine successions in the Middle Valley of the Tiber River. *Il Quat.* **2003**, *16*, 89–106.
25. Marra, F.; Florindo, F. The subsurface geology of Rome: Sedimentary processes, sea-level changes and astronomical forcing. *Earth Sci. Rev.* **2014**, *136*, 1–20. [[CrossRef](#)]
26. Milli, S. Depositional setting and high-frequency sequence stratigraphy of the Middle-Upper Pleistocene to Holocene deposits of the Roman Basin. *Geol. Romana* **1997**, *33*, 99–136.
27. Funciello, R.; Giuliani, R.; Marra, F.; Salvi, S. Superfici strutturali plio-quadernarie al margine sud-orientale del Distretto Vulcanico Sabatino. *Studi Geol. Camerti. Spec. CROP* **1991**, *11*, 301–304.
28. De Rita, D.; Funciello, R.; Parotto, M. *Geological Map of the Colli Albani Volcanic Complex, 1:50,000 Scale*; SELCA: Florence, Italy, 1988.
29. De Rita, D.; Faccenna, C.; Funciello, R.; Rosa, C. Structural and geological evolution of the Colli Albani volcanic district. In *The Volcano of the Alban Hills*; Trigila, R., Ed.; Tipografia SGS: Rome, Italy, 1995; pp. 33–71.
30. Barberi, F.; Buonasorte, G.; Cioni, R.; Fiordelisi, A.; Foresi, L.; Iaccarino, S.; Laurenzi, M.A.; Sbrana, A.; Vernia, A.; Villa, I.M. Plio-Pleistocene geological evolution of the geothermal area of Tuscany and Latium. *Mem. Descr. Carta Geol. It.* **1994**, *49*, 77–135.
31. Karner, D.B.; Marra, F.; Renne, P.R. The history of the Monti Sabatini and Alban Hills volcanoes: Groundwork for assessing volcanic-tectonic hazards for Rome. *J. Volcanol. Geotherm. Res.* **2001**, *107*, 185–219. [[CrossRef](#)]
32. Alfonsi, L.; Funciello, R.; Mattei, M.; Girotti, O.; Maiorani, A.; Preite Martinez, M.; Trudu, C.; Turi, B. Structural and geochemical features of the Sabina strike-slip fault (Central Apennines). *Boll. Soc. Geol. Ital.* **1991**, *110*, 217–230.
33. Faccenna, C. Structural and hydrogeological features of Pleistocene shear zones in the area of Rome (Central Italy). *Ann. Geofis.* **1994**, *37*, 121–133. [[CrossRef](#)]
34. Faccenna, C.; Funciello, R.; Mattei, M. Late Pleistocene N-S shear zones along the Latium Tyrrhenian margin: Structural characters and volcanological implications. *Boll. Geofis. Teor. Appl.* **1994**, *36*, 507–522.
35. Milli, S.; Mancini, M.; Moscatelli, M.; Stigliano, F.; Marini, M.; Cavinato, G.P. From river to shelf, anatomy of a high-frequency depositional sequence: The late Pleistocene to Holocene Tiber depositional sequence. *Sedimentology* **2016**, *63*, 1886–1928. [[CrossRef](#)]
36. Di Salvo, C.; Di Luzio, E.; Mancini, M.; Moscatelli, M.; Capelli, G.; Cavinato, G.P.; Mazza, R. GIS-based hydrostratigraphic modeling of the city of Rome (Italy): Analysis of the geometric relationships between a buried aquifer in the Tiber Valley and the confining hydrostratigraphic complexes. *Hydrogeol. J.* **2012**, *20*, 1549–1567. [[CrossRef](#)]
37. Minissale, A. Origin, transport and discharge of CO₂ in central Italy. *Earth Sci. Rev.* **2004**, *66*, 89–141. [[CrossRef](#)]
38. Kele, S.; Breitenbach, S.F.M.; Capezzuoli, E.; Meckler, A.N.; Ziegler, M.; Millan, I.M.; Kluge, T.; Deák, J.; Hanselmann, K.; John, C.M.; et al. Temperature dependence of oxygen- and clumped isotope fractionation in carbonates: A study of travertines and tufas in the 6–95 °C temperature range. *Geochim. Cosmochim. Acta* **2015**, *168*, 172–192. [[CrossRef](#)]
39. Chafetz, H.S.; Folk, R.L. Travertines: Depositional morphology and the bacterially constructed constituents. *J. Sediment. Petrol.* **1984**, *54*, 289–316.
40. Andrews, J.E.; Brasier, A.T. Seasonal records of climatic change in annually laminated tufas: Short review and future prospects. *J. Quat. Sci.* **2005**, *20*, 411–421. [[CrossRef](#)]
41. Claes, H.; Huysmans, M.; Soete, J.; Dirix, K.; Vassilieva, E.; Marques Erthal, M.; Vandewijngaerde, W.; Hamaekers, H.; Aratman, C.; Özkul, M.; et al. Elemental geochemistry to complement stable isotope data of fossil travertine: Importance of digestion method and statistics. *Sediment. Geol.* **2019**, *386*, 118–131. [[CrossRef](#)]
42. Huang, Y.-M.; Fairchild, I.J. Partitioning of Sr and Mg into calcite under karst-analogue experimental conditions. *Geochim. Cosmochim. Acta* **2001**, *65*, 47–62. [[CrossRef](#)]
43. Ihlenfeld, C.; Norman, M.D.; Gagan, M.K.; Drysdale, R.N.; Maas, R.; Webb, J. Climatic significance of seasonal trace element and stable isotope variations in a modern freshwater tufa. *Geochim. Cosmochim. Acta* **2003**, *67*, 2341–2357. [[CrossRef](#)]
44. Gabitov, R.I.; Sadekov, A.; Leinweber, A. Crystal growth rate effect on Mg/Ca and Sr/Ca partitioning between calcite and fluid: An in situ approach. *Chem. Geol.* **2014**, *367*, 70–82. [[CrossRef](#)]
45. Day, C.D.; Henderson, G.M. Controls on trace-element partitioning in cave-analogue calcite. *Geochim. Cosmochim. Acta* **2014**, *120*, 612–627. [[CrossRef](#)]
46. Jensen, D.L.; Boddum, J.K.; Tjell, J.C.; Christensen, T.H. The solubility of rhodochrosite (MnCO₃) and siderite (FeCO₃) in anaerobic aquatic environments. *Appl. Geochem.* **2002**, *17*, 503–511. [[CrossRef](#)]
47. Lisiecki, L.E.; Raymo, M.E. A Pliocene-Pleistocene stack of 57 globally distributed benthic $\delta^{18}O$ records. *Paleoceanography* **2005**, *20*, PA1003. [[CrossRef](#)]
48. Johnsen, S.J.; Clausen, H.B.; Dansgaard, W.; Fuhrer, K.; Gundestrup, N.; Hammer, C.U.; Iversen, P.; Jouzel, J.; Stauffer, B.; Steffensen, J.P. Irregular glacial interstadials recorded in a new Greenland ice core. *Nature* **1992**, *359*, 311–313. [[CrossRef](#)]

49. Dansgaard, W.; Johnsen, S.; Clausen, H.B.; Dahl-Jensen, D.; Gundestrup, N.S.; Hammer, C.U.; Hvidberg, C.S.; Steffensen, J.P.; Sveinbjörnsdóttir, A.E.; Jouzel, J.; et al. Evidence for general instability of past climate from a 250-kyr ice-core record. *Nature* **1993**, *364*, 218–220. [[CrossRef](#)]
50. Clark, P.U.; Dyke, A.S.; Shakun, J.D.; Carlson, A.E.; Clark, J.; Wohlfarth, B.; Mitrovica, J.X.; Hostetler, S.W.; McCabe, A.M. The last glacial maximum. *Science* **2009**, *325*, 710–713. [[CrossRef](#)] [[PubMed](#)]
51. Tzedakis, P.C.; Andrieu, V.; de Beaulieu, J.-L.; Birks, H.J.B.; Crowhurst, S.; Follieri, M.; Hooghiemstra, H.; Magri, D.; Reille, M.; Sadori, L.; et al. Establishing a terrestrial chronological framework as a basis for biostratigraphical comparisons. *Quat. Sci. Rev.* **2001**, *20*, 1583–1592. [[CrossRef](#)]
52. Spratt, M.; Lisiecki, L.E. A Late Pleistocene sea level stack. *Clim. Past* **2016**, *12*, 1079–1092. [[CrossRef](#)]

Disclaimer/Publisher’s Note: The statements, opinions and data contained in all publications are solely those of the individual author(s) and contributor(s) and not of MDPI and/or the editor(s). MDPI and/or the editor(s) disclaim responsibility for any injury to people or property resulting from any ideas, methods, instructions or products referred to in the content.